Articles in PresS. J Neurophysiol (February 13, 2013). doi:10.1152/jn.01043.2012

Title Page

Imaging light responses of retinal ganglion cells in the living mouse eye

Lu Yin[2], Ying Geng[2, 3], Fumitaka Osakada[4], Robin Sharma[2, 3], Ali H. Cetin[4], Edward M. Callaway[4], David R. Williams[2, 3], William H. Merigan[1, 2]

Flaum Eye Institute[1], Center for Visual Science[2], Institute of Optics[3], University of Rochester, Rochester, NY, USA

Systems Neurobiology Laboratory[4], Salk Institute for Biological Studies, La Jolla, CA, USA

Correspondence should be addressed to:
William H. Merigan
University of Rochester Medical Center
Box 314
Rochester, NY 14642
billm@cvs.rochester.edu

Running head: *In vivo* calcium imaging of mouse retinal ganglion cells

Journal: Journal of Neurophysiology, Innovative Methodology

Author Contributions:

L.Y., D.R.W. and W.H.M. designed the research, L.Y. performed the imaging experiments and analyzed the data, Y.G. designed and implemented the mouse adaptive optics instrumentation, R.S. and L. Y. modified the imaging system for this study, F.O. and E.M.C. developed the g-deleted rabies vector transporting G-CaMP3 gene, L.Y. made intracranial injections with advice from A.H.C., L.Y., D.R.W. and W.H.M. wrote the paper and all authors were involved in modifying it.

Abstract

This study reports development of a novel method for high resolution *in vivo* imaging of the function of individual mouse retinal ganglion cells (RGCs) that overcomes many limitations of available methods for recording RGC physiology. The technique combines insertion of a genetically encoded calcium indicator into RGCs with imaging of calcium responses over many days with FACILE (functional adaptive optics cellular imaging in the living eye). FACILE extends the most common method for RGC physiology, *in vitro* physiology, by allowing repeated imaging of the function of each cell over many sessions and by avoiding damage to the retina during removal from the eye. This makes it possible to track changes in the response of individual cells during morphological development or degeneration. FACILE also overcomes limitations of existing *in vivo* imaging methods, providing fine spatial and temporal detail, structure – function comparison and simultaneous analysis of multiple cells.

Keywords: retinal ganglion cells, *in vivo* adaptive optics imaging, calcium imaging

Introduction

Available methods for examining the physiology of retinal ganglion cells (RGCs) have marked limitations, which are resolved by the novel *in vivo* imaging method described here. Existing *in vivo* methods study cells in a relatively unperturbed state, but the physical challenge of recording within the eye often limits recording to a small number of cells (e.g., Martin et al. 2001), and repeated study of individual cells is not possible. *In vitro* recording is a highly efficient approach, imaging or recording electrophysiological responses from many cells simultaneously (e.g., Borghuis et al. 2011; Chichilnisky and Kalmar 2002), but it has two major limitations. It does not permit long term study of the same retinal neurons and circuitry over time, for example the study of how neurons degenerate or how they change during development. Also, *in vitro* methods do not avoid possible artifacts due to retina removal itself, for example the effect of cutting the axons of ganglion cells (Lukas et al. 2009; Mandolesi et al. 2004).

Here we demonstrate an *in vivo* imaging method, FACILE (functional adaptive optics cellular imaging in the living eye), that can repeatedly image the light response of ganglion cells in eyes of living mice. This method shares the advantages of other *in vivo* techniques in studying retinal cells in an intact state and it can track the response of individual cells over days or weeks. Like other imaging methods, FACILE permits the study of many cells simultaneously, but unlike low resolution imaging (Prilloff et al. 2010; Sabel et al. 1997), it provides both subcellular resolution and high sensitivity. Fluorescent adaptive optics (AO) imaging has previously been used to image the morphology of retinal ganglion cells expressing fluorescent protein in living rodent eyes, and characterize their dendritic stratification (Geng et al. 2012; Geng et al. 2009). Here, to study ganglion cell physiology, we expressed the genetically encoded calcium indicator (GECI), G-CaMP3 (Tian et al. 2009), in retinal ganglion cells, and tracked the calcium response of individual cells to visual stimuli. A challenge of *in vivo* fluorescent imaging is that it uses

visible light that strongly light adapts the retina. For example, in this study the excitation wavelength was 488 nm, which is close to the peak sensitivity of mouse middle-wavelength sensitive (M) cone opsin, and rhodopsin (Jacobs et al. 2004; Lyubarsky et al. 2004; Lyubarsky et al. 1999). In order to separate visual activation from response to the imaging light, we used ultraviolet (UV) light (365 nm) to stimulate the retina thus selectively activating the short-wavelength sensitive (S) cone opsin, which activates most retinal ganglion cells (Wang et al. 2011).

Because *in vivo* imaging is intrinsically photon-limited, we used a viral-vector mediated gene delivery that leads to a high level of G-CaMP3 expression in cells, without damaging the cells. The rabies vector produced intense G-CaMP3 expression in individual ganglion cells without non-specific background expression, which improved the signal to noise (SNR) of imaging. As described below, rabies mediated G-CaMP3 expression produced stable physiological responses in cells over the first 4 to 8 days of imaging, which then declined as the cells began to degenerate.

Materials and Methods

Intracranial injection of rabies vector

Rabies vector was produced in the laboratory of Dr. Edward M. Callaway (Salk Institute for Biological Study, San Diego, CA, USA). In brief, G-deleted rabies viruses are generated in B7GG cells, concentrated by two rounds of centrifugation, and titrated in HEK293t cells as described previously (Osakada et al. 2011). The titers of the viruses used in this study were 4.8-8.0 x 10^8 infectious units/ml. The injection procedure was as described previously (Cetin et al. 2006), and followed the guidelines of Biosafety Level 2. Typical coordinates of injections into superior colliculus were 3.8 mm posterior to Bregma, 1.0 mm lateral, at two depths of 1.4 and 1.7 mm (Keith B.J. Franklin 2007), and injection volume was 0.5 µl at each depth. During injections the cornea was lubricated with GenTeal (Bausch & Lomb, Rochester, NY, USA) to prevent cataract formation. AO imaging began four days after injection to allow recovery from surgery, as well as ganglion cell expression of G-CaMP3. Wild-type C57BL/6J mice of both sexes were used. All animal procedures were conducted according to the ARVO Statement for the Use of Animals and the guidelines of the Office of Laboratory Animal Care at the University of Rochester. The protocol was approved by the University Committee on Animal Resources of the University of Rochester.

Adaptive optics imaging

Prior to AO imaging, the retinal distribution of transduced ganglion cells was identified on low-resolution fluorescent images of the mouse retina, obtained with a fundus camera (Micron III, Phoenix Research Laboratories, Inc, Pleasanton, CA, USA), or confocal scanning laser ophthalmoscope (SLO) (Spectralis HRA, Heidelberg Engineering, Germany). FACILE was done with the mouse fluorescence adaptive optics SLO built at the University of Rochester. A detailed description of this system, and characterization of its performance for imaging various

retinal structures has been reported elsewhere (Geng et al. 2012). Briefly, during imaging, we captured two channels of images simultaneously: a reflectance image of the retinal structure (e.g., vessels in the inner retina), using infrared light with center wavelength 790 nm, and a fluorescence image of the G-CaMP3 expressing ganglion cells (excitation: 488 nm, and emission: 525 ± 17.5 nm) (FF01-520/35-25, Semrock, Rochester, NY, USA). Infrared (IR) light of 850 nm was also used for wavefront sensing to correct the optical aberrations of the mouse eye. All imaging lights, 488, 790 and 850 nm, were scanned over a 6 × 5 degree rectangular region on the retina, and AO images were taken over a central 5 x 5 degree square, where illumination was more uniform. The intensities of the imaging lights at pupil were around 100 μW (488 nm), 150 μW (790 nm) and 25 μW (850 nm).

Eye motion was calculated from high SNR reflectance images of retinal structure (e.g., vasculature), and the motion correction applied to both channels. Images of both channels were captured at 25 Hz. The gain of the fluorescence channel was set to fully utilize the dynamic range of the system, with only a small percent of pixels being saturated. For navigation across the retina the retinal vasculature visible in AO reflectance was compared to low resolution, large field fundus images.

Presentation of UV light

The primary visual stimulus was 365 nm ultraviolet light. The UV light was generated by an LED that produced a peak wavelength of 365 nm (M365L2-UV, Thorlabs, Newton, NJ, USA), and was presented to the eye in Maxwellian view over a circular region of ~ 24 degree diameter on the retina. The intensity of the UV light at pupil was 20 μW.

Visual impact of imaging and visual stimulation lights

To compare the visual impact on photoreceptors of the various imaging and stimulation lights, we calculated isomerization rates for mouse M- and S- pigments and rhodopsin using

methods described by Naarendorp (2010) (see also, Wang et al. 2011) (Fig. 1*A*,*B*). The spectral sensitivities followed the template developed by Govardovskii et al. (2000) using λ_{max}s of 508 nm, 360 nm and 498 nm (Jacobs et al. 2004; Lyubarsky et al. 2004; Lyubarsky et al. 1999). Pigment self-screening was calculated based on inner segment lengths of 13.4 um for cones and 24 um for rods measured by Carter-Dawson and LaVail (1979), and an axial specific density of 0.015 um^{-1} for cones and 0.019 um^{-1} for rods (Naarendorp et al. 2010). The end-on collecting area of mouse rods and cones were 0.85 μm^2 and 1 μm^2 (Naarendorp et al. 2010). Pre-retinal absorption of the mouse eye was estimated from Henriksson, et al. (2010). To simply the calculation, all light sources were treated as monochromatic light, with all the power at the spectral peak. To estimate the bleaching effect of imaging lights, we assumed a total 7.4 $\log_{10}$ pigments in a M cone (Fu 2011), estimated from cone outer segment volume of 14 μm^3 (Carter-Dawson and LaVail 1979) and a pigment concentration of ~ 3 mM (Harosi 1975). Psychophysics Toolbox extensions (Brainard 1997; Pelli 1997) were used for calculating isomerization rates. Although the UV stimulus light produced visible autofluorescence at the contact lens surface, the confocal AO system eliminated this fluorescence signal.

Experimental procedure

The primary stimulus used to activate ganglion cells was an 8 sec steady presentation of 365 nm (UV) light, which alternated with 8 sec of no UV light. For a few measures other stimuli were used; 1 sec steady presentation of UV light, alternating with 15 sec of no UV light or onset of the 488 nm imaging field.

To minimize retinal exposure to blue light, the 488 nm imaging light was extinguished between each imaging block. At each retinal location, an imaging block was of ~ 3 min duration, with at least 1 min between recording blocks. Baseline fluorescence generally

decreased over the first 30 sec of each block, thus data analysis excluded the initial 30 sec of each block.

Measurement of fluorescence intensity of ganglion cell somas

Fluorescent measurements were made from motion-corrected (registered) fluorescent videos, using Fiji (Schindelin et al. 2012), a distribution package of ImageJ (Rasband, W.S., ImageJ, U. S. National Institutes of Health, Bethesda, Maryland, USA, http://imagej.nih.gov/ij/, 1997-2011). For each registered fluorescent video, round or ellipsoidal regions of interests (ROIs) were placed on each ganglion cell soma identified in the summed image of that video (see Fig. 2). As a measure of background, a rectangular ROI larger than a typical ganglion cell soma was placed at a location where there were no visible ganglion cell somas. Fluorescence intensity was measured within ROIs for each frame of the video, generating a temporal sequence of fluorescence intensity for each identified ganglion cell soma.

To improve the signal-noise-ratio of the measurement (as illustrated in Fig. 2*B*, left panel), we binned 10 successive samples, reducing the temporal sampling rate from 25 Hz to 2.5 Hz, a rate that is fast relative to the calcium response of ganglion cells. A time stamp was recorded for every video frame during image capture, in order to correctly align each frame with the timing of stimulus presentation.

Measurement of peak response from normalized fluorescence

We calculated fluorescence response (ratio F/F_0), by normalizing measured fluorescence (F) of each stimulus cycles to the mean baseline value (F_0) obtained from the time preceding the onset of the UV flash (2 sec to 0.4 sec before onset). Time of the peak response was identified from smoothed data with a 3-sample moving boxcar average, and the peak response amplitude was determined as the mean of three consecutive time points statistically different from baseline ($F/F_0 = 1$), using a one-tailed t-test. All data analysis used MATLAB (MathWorks, Natick, MA).

Evaluation of light safety with repeated imaging

Total light exposure included the imaging lights, primarily 488 and 790 nm, and the visual stimulation light, 365 nm. Exposure to the imaging lights did not exceed 1.7 times the American National Standards Institute (American National Standard for the Safe Use of Lasers ANSI Z136.1-2007) maximum permissible exposure (MPE) for human retina (Delori et al. 2007) scaled by the ratio of the numerical aperture (NA) of human to mouse eyes ($NA_{Human}^2/NA_{Mouse}^2$ = 0.2) (Geng et al. 2012). This exposure level was considered unlikely to be damaging, given that the MPE is set 10 fold below minimum damage thresholds to ensure safety. Maximum radiant exposure to UV light for each eye, each day was 0.18 – 1.02 J/cm^2. This value cannot be compared to human safety limits since there is no MPE standard for UV light, but this light level is of concern, given that it approaches the value that has been shown to produce retinal damage in rat (Busch et al. 1999; Gorgels and van Norren 1995; van Norren and Gorgels 2011). Despite this concern, no photoreceptor alteration or loss was found in AO imaging at any retinal location on any of the imaging sessions over 7 days, nor was there any visible change in cornea or lens. Our previous studies have demonstrated that AO imaging is a highly sensitive indicator of light damage, showing retinal changes in monkey retina at light levels well below ANSI MPE standards for light safety (Morgan et al. 2008).

Results

Combining calcium imaging with *in vivo* fluorescent AO imaging

This study combined a previously described method for high-resolution *in vivo* adaptive optics imaging of reflectance and fluorescence signals from mouse retina (Geng et al. 2012), with insertion of the genetically encoded calcium indicator, G-CaMP3 into RGCs (Tian et al. 2009). G-CaMP3 was expressed in mouse RGCs by injecting glycoprotein-deleted rabies vector (Osakada et al. 2011), carrying the G-CaMP3 gene, intracranially into mouse superior colliculus, producing RGC transduction in a few days. The apparatus and method for adaptive optics imaging was as previously described (Geng et al. 2012) with the following exceptions. The imaging laser in the present study was 488 nm rather than 514 nm, chosen to match the excitation of G-CaMP3, and lower laser intensities were used in this study in order to maintain safe light levels during the extended imaging needed to characterize physiological responses (see *Materials and Methods*).

Visual stimuli were 488 nm (blue) or 365 nm (UV)

To excite retinal neurons we initially used the onset of the 488 nm (blue) imaging field, a wavelength near the peak sensitivities of both mouse M cones and rods (Figs. 1*A* and 2*A*). However, to minimize interactions between the stimulation and imaging light, most measurements in this study were made of responses to 365 nm (UV) light (Figs. 1*A* and 2*B*), obtained in the presence of constant 488 nm illumination. As shown in Figure 1*A*, 365 nm light is near the peak sensitivity of mouse S cones (Jacobs and Rowe 2004; Lyubarsky et al. 1999; Nikonov et al. 2006), and activates both S cones, and the many cones that co-express M- and S-opsins (Applebury et al. 2000; Haverkamp et al. 2005; Jacobs and Williams 2007; Rohlich et al. 1994; Wang et al. 2011). To reduce the visual impact of the 488 nm imaging light on S cones,

the intensity of the UV stimulus was set approximately 3 $\log_{10}$ units above that of the 488 nm fluorescence imaging light (Fig. 1*B*).

Calcium responses to brief stimuli

We examined the time course of calcium responses to brief stimuli, initially to onset of the 488 nm imaging field. Figure 2*A* illustrates the G-CaMP3 response of a ganglion cell in the living mouse eye to onset of the 488 nm imaging light. The response (blue curve) showed a quick rise to peak, followed by a slower decay to baseline within 10 sec. This response demonstrates that the 488 nm imaging light activates retinal neurons, suggesting that calcium responses might best be understood if the 488 nm light was held constant. The right panel of Figure 2*A* shows the method used to determine calcium responses on a summed fluorescence image of ganglion cells expressing G-CaMP3. To determine the time course of G-CaMP3 fluorescence, we measured mean fluorescence intensity within oval regions of interest (ROI) at the selected ganglion cell soma (Fig. 2*A*, white oval in the right panel).

To separate the effects of visual stimulation from activation by the imaging field, we kept the 488 imaging field constant and measured the calcium response to a brief pulse of UV light. Figure 2*B* shows the time course of the calcium response to a 1 sec pulse of UV light, measured from the ganglion cell soma within the white oval ROI on the right panel. The fluorescence intensity (Fig. 2*B*, red curve) rises slowly, peaking at approximately 2 seconds and returning to baseline approximately 4 seconds after stimulus onset.

Calcium responses to UV stimuli of longer duration

Following the above measurement of responses to brief stimuli, the remaining data in this study were collected using 8 sec presentation of the UV stimulus, in order to reveal both transient and sustained calcium responses. Figure 3 shows examples of fluorescent responses to UV stimuli measured on day 6 following rabies injections. The temporal profile of responses

varied across cells, increasing in some and decreasing in others. For cells having increased responses, the responses of some cells continued to increase or plateaued as long as the UV stimulus was present (e.g., Fig. 3*A*, top panel and Fig. 3*B*, panels in the top row), while responses of other cells peaked early during the 8-second UV stimulus and then declined (e.g., Fig. 3*B*, the first, third and fourth panels from left in the second row). For all cells with a decreased response, responses generally continued to decrease as long as the UV stimulus was present. However, after UV stimulus offset, the response of some cells recovered to baseline level rapidly (e.g., Fig. 3*A*, bottom panel and Fig. 3*B*, middle panel in the third row and the first panel from left in the fourth row), while the response of other cells recovered more slowly (e.g., Fig. 3*B*, the first and third panels from left in the third row). To estimate the main peak response amplitude across ganglion cell population, we quantified peak responses of 60 imaged cells measured on day 6 (see *Appendix*). 11 out of the 60 cells showed statistically significant increase in fluorescence. 41 out of the 60 cells showed statistically significant decrease in fluorescence. The mean amplitude of increased fluorescence was 0.4 ± 0.4 (SD), which was approximately 3 fold greater than that of decreased fluorescence: 0.15 ± 0.04 (SD).

Calcium responses of ganglion cells across time after rabies injection

To evaluate the value of FACILE methodology for chronic study of neuronal responses, we examined the calcium response of individual ganglion cells across multiple days, during which the cells degenerated. Figure 4*A* shows repeated imaging on days 4, 6, 8 and 10 of two clusters of G-CaMP3 expressing ganglion cells in the retinas of two different mice. The total number of transduced ganglion cells was highest around day 6 (Fig. 4*A*, bottom panels). To assess the consistency of cell responses over multiple days, normalized responses of selected cells were shown in Figure 4*B* (see Fig. 3 also, for cells identified with same numbers). A transduced ganglion cell was typically visible for at least three of the time points, and different

cells initially became visible on different days. For example, cells 1- 4 were visible on days 4 - 8, whereas cell 5 was visible on day 6-10 (Fig. 4*A*). For cells showing increased fluorescence to visual stimulation, responses were typically stable for two time points, then greatly decreased at the third time point (e.g., cells 1- 3 in Fig. 4*B*), whereas those showing decreased fluorescence often remained relatively stable until they could no longer be imaged (cells 7 - 12 in Fig. 4*B*).

Discussion

This study demonstrated a novel method for the repeated *in vivo* imaging of calcium responses of individual retinal ganglion cells in the mouse eye. It utilized an adaptive optics imaging system (Geng et al. 2012; Gray et al. 2006; Gray et al. 2008) to obtain high-resolution images of fluorescing cells in retina despite the challenges of low fluorescence levels and eye movements. We employed an UV light source that activates the S-cone opsin in order to measure ganglion cell responses in the presence of the blue imaging laser, which also excites M-cone opsin and rhodopsin. Correction of optical aberrations by the adaptive optics system permitted imaging of the subcellular structure (soma, proximal dendrites) of ganglion cells (Fig. 2*A*,*B*, right panels). Finally, the level of both imaging and stimulation light were kept low to avoid light damage that would compromise the repeated imaging of cells. This is the first report of high-resolution *in vivo* imaging of the light responses of individual retinal ganglion cells, and shows imaging of calcium responses of ganglion cells at temporal and spatial resolutions comparable to those used in similar *in vitro* studies (Borghuis et al. 2011; Briggman and Euler 2011; Weitz et al. 2013; Zariwala et al. 2012). As described above, important advantages of the FACILE method are simultaneous, high-resolution *in vivo* study of numerous cells, repeated imaging of single retinal cells over a long time, and the ability to relate the physiology of recorded cells to their morphology. The high axial resolution of FACILE can distinguish RGC cell types on the basis of their branching level within the inner plexiform layer (Geng et al. 2012). A major limitation of FACILE imaging of calcium is poor temporal resolution compared to electrophysiology. However, in the future, we could avoid the inherently slow calcium response by using voltage-sensitive indicators (Mutoh et al. 2012). Other limitations of the present method can be reduced by incorporating methodologies described below in future directions.

Comparison with prior *in vitro* calcium imaging studies of RGCs

The calcium response of ganglion cells to light stimulation has previously been recorded with *in vitro* preparations (Borghuis et al. 2011; Briggman and Euler 2011; Zariwala et al. 2012). These studies used either a calcium indicator dye, Oregon Green BAPTA (OGB), or a genetically encoded calcium indicator, G-CaMP3, imaged with a two-photon laser. Briggman and Euler (2011) studied the calcium response of mouse ganglion cells to 1.5 second presentation of a 420 nm and 580 nm spot that ranged in diameter from 50 µm to 800 µm. Responses to a 800 µm spot (their Fig. 2*A*), the condition most similar to that used in the present study, showed increased or decreased fluorescent response similar to that seen in Figure 3 in the present study. Borghuis et al. (2011) studied the calcium responses of mouse ganglion cell to 2 sec presentation of a full-field 458 nm stimulus (their Fig. 6*B*), and also showed increased or decreased responses to light in some cells similar to that seen in Figure 3 of this study.

Both Borghuis et al. (2011) and Briggman and Euler (2011) showed cells with clear OFF responses, i.e. fluorescence increase above baseline level to light off. While many cells in our study showed decreased responses during the 8-sec UV flash presentation (Fig. 3), none showed increased fluorescence above baseline after the 8-sec UV flash was extinguished. The ~ 24 degree UV spot used in our study was much larger than the optimal 10 degree spot diameter for mouse ganglion cells (Schmucker and Schaeffel 2004; Stone and Pinto 1993), which can greatly reduce OFF responses of OFF-center ganglion cells (Sagdullaev and McCall 2005). Thus, although our responses appear consistent with those reported by Briggman and Euler (2011) for spot diameter of 800 µm, smaller spot sizes will be needed to demonstrate unequivocal OFF responses.

Future directions for FACILE

The FACILE method described here can be extended to additional applications by slight changes in calcium indicators, visual stimuli, imaging methods and even different species. Long-term retinal changes could be examined over weeks to months by the use of less damaging methods for inserting GECIs into retinal cells than the rabies virus used here. Precisely focused patterned stimuli, generated with the adaptive optics system, can be used to map receptive fields with high precision. The method is currently being extended to non-human primates, which offer an animal model of retinal function and dysfunction that is closely related to human retina. Different imaging modalities will greatly extend the capabilities of the FACILE method. For example, the use of fluorescence resonance energy transfer (FRET) based sensors can provide both ratiometric calcium imaging and structural imaging, and extend the method towards studying fine scale molecular interactions. Furthermore, multiphoton methods (Hunter et al. 2011) will permit non-invasive FACILE imaging of many compounds involved in the retinoid cycle, thus potentially extending the approach to the human retina.

335 ## *Appendix*

336 ### Quantification of calcium responses across the RGC population

337 On day 6 after rabies injection, we imaged the calcium responses of total 60 transduced

338 cells from 6 retinal locations in 5 mouse eyes. Figure 5 summarizes the measured peak response

339 (F/F_0) and time to peak across population.

340

Acknowledgements

We thank Jennifer Strazzeri and Stacy Ruvio for assistance with surgery, Jennifer Norris for assistance with data processing, William Fischer, Rachel Hollar, and Lee Anne Schery for assistance with cSLO, or AO imaging, Kamran Ahmad for assistance with imaging software programming and hardware interface, Jennifer Hunter for assistance with light safety calculations and Tracy Bubel for assistance with histology. Loren Looger supplied the G-CaMP3 plasmid and provided advice on its use.

Grants

This work was supported by NIH research grants-EY019375, EY021166, EY004367, BRP-EY014375, and NDC 5PN2EY018241; NIH Training Grant-EY07125; NIH Core Grant-EY001319.

Disclosures

DRW has license agreements for adaptive optics technology with Canon and Physical Sciences and consults for GlaxoSmithKelin and Pfizer. He also has an SBIR grant on development of novel adaptive optics technology with Polgenix.

All other authors declare no competing financial interests.

Figure Captions

Figure 1. Spectral configuration of the imaging lights and retinal visual stimulation, and their visual impact.

A. Spectral configuration. Peak wavelengths of the imaging lights for fluorescence imaging and visual stimulation compared to the normalized spectral sensitivity of mouse photoreceptors, corrected for self-screening. S cones are much less sensitivity to 488 nm imaging light than the 365 nm visual stimulation light.

B. Relative activation of photopigments by the different light sources. During imaging, S cones were activated well within their normal operating range by the 365 nm UV light (gray bar; 7.4 $\log_{10}$ *Rh**/cone/s), but much less affected by the 488 nm imaging light (dark bar; 4.4 $\log_{10}$ *Rh**/cone/s), as well as the 790 nm reflectance imaging light or the 850 nm wavefront sensing light (not shown). However, M pigments were strongly isomerized by the 488 imaging light (9.6 $\log_{10}$ *Rh**/cone/s), and are effectively bleached within a few seconds (see *Materials and Methods*). We could not directly calculate the isomerization rates produced by IR lights used for reflectance imaging and wavefront sensing, which should be far less than that calculated for a 700 nm light of similar power (200 μW at pupil; light gray bar). The horizontal line corresponds to an isomerization rate of 5200 Rh*/photoreceptor/s, and was used to visualize the start of photopic vision in mouse (Naarendorp et al. 2010; Wang et al. 2011), where rod saturation begins.

Figure 2. Time course of fluorescence response of ganglion cells to relatively transient visual stimuli.

380 *A*. Single calcium response of one ganglion cell to the onset of the 488 nm imaging field
381 (left edge of the gray rectangle). G-CaMP3 fluorescence (F/F_0) was calculated from intensity
382 measurement from the ganglion cell soma shown in the AO image on the left, within the region
383 of interests (white). Because the large amplitude of response can be clearly shown without
384 binning, data was plotted at 25 Hz. Scale bar = 20 μm.

385 *B*. Mean and individual calcium response of one ganglion cell to 1 sec duration pulses of
386 UV light (gray rectangle). Mean response (red) was calculated from 18 individual responses
387 (gray line). Data was plotted at 2.5 Hz. Binning and averaging of individual responses was done
388 to improve SNR, so that small changes in fluorescence intensity can be revealed. The vertical
389 dotted line shows the calculated peak fluorescence response. Scale bar = 20 μm.

390

391 **Figure 3.** Time course of fluorescent responses of ganglion cells to 8 sec duration pulses of UV
392 light (gray rectangle), showing either increased or decreased fluorescence after stimulus onset.

393 *A* and *B*. Responses from 16 ganglion cells are shown, measured on day 6 after rabies
394 injection. Red curves show the mean of individual responses (gray; 2.5 Hz sampling rate, or 0.4
395 sec temporal resolution). Maximal peak positive or negative response was shown in *A*, while the
396 other responses are shown in *B*, in difference scales for the y-axis. Vertical dashed lines show
397 the time of peak positive or negative response. The numbering of cells is the same as in Figure
398 4*A*.

399

400 **Figure 4.** Tracking rabies transduction and light responses of identified ganglion cells across
401 multiple days.

A. AO images of rabies transduced ganglion cells at two retinal locations in two eyes of two mice at 4, 6, 8 and 10 days after rabies injection, showing the time course of G-CaMP3 expression. Peak density of rabies transduced ganglion cells was between day 6 and 8, but by day 10, somas of many of the transduced ganglion cells were not visibly fluorescent, indicating cellular degeneration. Scale bar = 20 μm.

B. Normalized light responses to UV light of ganglion cells numbered in *A* across time. Responses ($\Delta F/F_0$) of each cell were normalized to the highest peak response amplitude. Mean responses are color-coded: black = day 4, red = day 6, green = day 8 and blue = day 10. The dotted gray line shows baseline of $\Delta F/F_0 = 0$.

Figure 5. Peak response (F/F_0) and time to peak of imaged ganglion cells on day 6 after rabies injection.

A. Scatter plot of peak response amplitude versus time to peak of the 52 out of 60 imaged cells from 6 locations in 5 mouse eyes that showed statistically significant peak responses. Cells with increased fluorescence to the UV stimulus are shown in red (± SE) and those with decreased fluorescence in green (± SE). The horizontal dashed line is the baseline of $F/F_0 = 1$, and the vertical dashed line is the end of the 8-second UV stimulus. Eight cells showed no statistically significant response, and were not shown. Y-axis is in $\log_{10}$ scale.

B. Histogram of the peak response amplitude. Mean increased fluorescence change ($\Delta F/F_0$) was 0.4 ± 0.4 (SD) and decreased fluorescence change was 0.15 ± 0.04 (SD). Bin width is 0.1. The horizontal dotted line is the baseline of $F/F_0 = 1$. Y-axis is in $\log_{10}$ scale.

C. Histogram of the time to peak. Bin width is 0.5 sec. The vertical dotted line shows offset of the UV flash.

425

References

Applebury ML, Antoch MP, Baxter LC, Chun LL, Falk JD, Farhangfar F, Kage K, Krzystolik MG, Lyass LA, and Robbins JT. The murine cone photoreceptor: a single cone type expresses both S and M opsins with retinal spatial patterning. *Neuron* 27: 513-523, 2000.

Borghuis BG, Tian L, Xu Y, Nikonov SS, Vardi N, Zemelman BV, and Looger LL. Imaging light responses of targeted neuron populations in the rodent retina. *J Neurosci* 31: 2855-2867, 2011.

Brainard DH. The Psychophysics Toolbox. *Spatial vision* 10: 433-436, 1997.

Briggman KL, and Euler T. Bulk electroporation and population calcium imaging in the adult mammalian retina. *J Neurophysiol* 105: 2601-2609, 2011.

Busch EM, Gorgels TG, and van Norren D. Temporal sequence of changes in rat retina after UV-A and blue light exposure. *Vision Res* 39: 1233-1247, 1999.

Carter-Dawson LD, and LaVail MM. Rods and cones in the mouse retina. I. Structural analysis using light and electron microscopy. *J Comp Neurol* 188: 245-262, 1979.

Cetin A, Komai S, Eliava M, Seeburg PH, and Osten P. Stereotaxic gene delivery in the rodent brain. *Nat Protoc* 1: 3166-3173, 2006.

Chichilnisky EJ, and Kalmar RS. Functional asymmetries in ON and OFF ganglion cells of primate retina. *J Neurosci* 22: 2737-2747, 2002.

Delori FC, Webb RH, and Sliney DH. Maximum permissible exposures for ocular safety (ANSI 2000), with emphasis on ophthalmic devices. *J Opt Soc Am A Opt Image Sci Vis* 24: 1250-1265, 2007.

Fu Y. Phototransduction in Rods and Cones. In: *Webvision: The Organization of the Retina and Visual System*, edited by Kolb H, Nelson R, Fernandez E, and Bryan J. Salt Lake City: 2011.

449 **Geng Y, Dubra A, Yin L, Merigan WH, Sharma R, Libby RT, and Williams DR**. Adaptive
450 optics retinal imaging in the living mouse eye. *Biomedical optics express* 3: 715-734, 2012.

451 **Geng Y, Greenberg KP, Wolfe R, Gray DC, Hunter JJ, Dubra A, Flannery JG, Williams**
452 **DR, and Porter J**. In vivo imaging of microscopic structures in the rat retina. *Invest Ophthalmol*
453 *Vis Sci* 50: 5872-5879, 2009.

454 **Gorgels TG, and van Norren D**. Ultraviolet and green light cause different types of damage in
455 rat retina. *Invest Ophthalmol Vis Sci* 36: 851-863, 1995.

456 **Govardovskii VI, Fyhrquist N, Reuter T, Kuzmin DG, and Donner K**. In search of the visual
457 pigment template. *Vis Neurosci* 17: 509-528, 2000.

458 **Gray DC, Merigan W, Wolfing JI, Gee BP, Porter J, Dubra A, Twietmeyer TH, Ahamd K,**
459 **Tumbar R, Reinholz F, and Williams DR**. In vivo fluorescence imaging of primate retinal
460 ganglion cells and retinal pigment epithelial cells. *Opt Express* 14: 7144-7158, 2006.

461 **Gray DC, Wolfe R, Gee BP, Scoles D, Geng Y, Masella BD, Dubra A, Luque S, Williams**
462 **DR, and Merigan WH**. In vivo imaging of the fine structure of rhodamine-labeled macaque
463 retinal ganglion cells. *Invest Ophthalmol Vis Sci* 49: 467-473, 2008.

464 **Harosi FI**. Absorption spectra and linear dichroism of some amphibian photoreceptors. *The*
465 *Journal of general physiology* 66: 357-382, 1975.

466 **Haverkamp S, Wassle H, Duebel J, Kuner T, Augustine GJ, Feng G, and Euler T**. The
467 primordial, blue-cone color system of the mouse retina. *J Neurosci* 25: 5438-5445, 2005.

468 **Henriksson JT, Bergmanson JP, and Walsh JE**. Ultraviolet radiation transmittance of the
469 mouse eye and its individual media components. *Exp Eye Res* 90: 382-387, 2010.

Hunter JJ, Masella B, Dubra A, Sharma R, Yin L, Merigan WH, Palczewska G, Palczewski K, and Williams DR. Images of photoreceptors in living primate eyes using adaptive optics two-photon ophthalmoscopy. *Biomed Opt Express* 2: 139-148, 2011.

Jacobs GH, and Rowe MP. Evolution of vertebrate colour vision. *Clin Exp Optom* 87: 206-216, 2004.

Jacobs GH, and Williams GA. Contributions of the mouse UV photopigment to the ERG and to vision. *Doc Ophthalmol* 115: 137-144, 2007.

Jacobs GH, Williams GA, and Fenwick JA. Influence of cone pigment coexpression on spectral sensitivity and color vision in the mouse. *Vision Res* 44: 1615-1622, 2004.

Keith B.J. Franklin GP. *The Mouse Brain in Stereotaxic Coordinates*. Academic Press, 2007.

Lukas TJ, Wang AL, Yuan M, and Neufeld AH. Early cellular signaling responses to axonal injury. *Cell communication and signaling : CCS* 7: 5, 2009.

Lyubarsky AL, Daniele LL, and Pugh EN, Jr. From candelas to photoisomerizations in the mouse eye by rhodopsin bleaching in situ and the light-rearing dependence of the major components of the mouse ERG. *Vision Res* 44: 3235-3251, 2004.

Lyubarsky AL, Falsini B, Pennesi ME, Valentini P, and Pugh EN, Jr. UV- and midwave-sensitive cone-driven retinal responses of the mouse: a possible phenotype for coexpression of cone photopigments. *J Neurosci* 19: 442-455, 1999.

Mandolesi G, Madeddu F, Bozzi Y, Maffei L, and Ratto GM. Acute physiological response of mammalian central neurons to axotomy: ionic regulation and electrical activity. *FASEB journal : official publication of the Federation of American Societies for Experimental Biology* 18: 1934-1936, 2004.

Martin PR, Lee BB, White AJ, Solomon SG, and Ruttiger L. Chromatic sensitivity of ganglion cells in the peripheral primate retina. *Nature* 410: 933-936, 2001.

Morgan JI, Hunter JJ, Masella B, Wolfe R, Gray DC, Merigan WH, Delori FC, and Williams DR. Light-induced retinal changes observed with high-resolution autofluorescence imaging of the retinal pigment epithelium. *Invest Ophthalmol Vis Sci* 49: 3715-3729, 2008.

Mutoh H, Akemann W, and Knopfel T. Genetically engineered fluorescent voltage reporters. *ACS chemical neuroscience* 3: 585-592, 2012.

Naarendorp F, Esdaille TM, Banden SM, Andrews-Labenski J, Gross OP, and Pugh EN, Jr. Dark light, rod saturation, and the absolute and incremental sensitivity of mouse cone vision. *J Neurosci* 30: 12495-12507, 2010.

Nikonov SS, Kholodenko R, Lem J, and Pugh EN, Jr. Physiological features of the S- and M-cone photoreceptors of wild-type mice from single-cell recordings. *The Journal of general physiology* 127: 359-374, 2006.

Osakada F, Mori T, Cetin AH, Marshel JH, Virgen B, and Callaway EM. New rabies virus variants for monitoring and manipulating activity and gene expression in defined neural circuits. *Neuron* 71: 617-631, 2011.

Pelli DG. The VideoToolbox software for visual psychophysics: transforming numbers into movies. *Spatial vision* 10: 437-442, 1997.

Prilloff S, Fan J, Henrich-Noack P, and Sabel BA. In vivo confocal neuroimaging (ICON): non-invasive, functional imaging of the mammalian CNS with cellular resolution. *Eur J Neurosci* 31: 521-528, 2010.

Rohlich P, van Veen T, and Szel A. Two different visual pigments in one retinal cone cell. *Neuron* 13: 1159-1166, 1994.

Sabel BA, Engelmann R, and Humphrey MF. In vivo confocal neuroimaging (ICON) of CNS neurons. *Nat Med* 3: 244-247, 1997.

Sagdullaev BT, and McCall MA. Stimulus size and intensity alter fundamental receptive-field properties of mouse retinal ganglion cells in vivo. *Vis Neurosci* 22: 649-659, 2005.

Schindelin J, Arganda-Carreras I, Frise E, Kaynig V, Longair M, Pietzsch T, Preibisch S, Rueden C, Saalfeld S, Schmid B, Tinevez JY, White DJ, Hartenstein V, Eliceiri K, Tomancak P, and Cardona A. Fiji: an open-source platform for biological-image analysis. *Nat Methods* 9: 676-682, 2012.

Schmucker C, and Schaeffel F. A paraxial schematic eye model for the growing C57BL/6 mouse. *Vision Res* 44: 1857-1867, 2004.

Stone C, and Pinto LH. Response properties of ganglion cells in the isolated mouse retina. *Vis Neurosci* 10: 31-39, 1993.

Tian L, Hires SA, Mao T, Huber D, Chiappe ME, Chalasani SH, Petreanu L, Akerboom J, McKinney SA, Schreiter ER, Bargmann CI, Jayaraman V, Svoboda K, and Looger LL. Imaging neural activity in worms, flies and mice with improved GCaMP calcium indicators. *Nat Methods* 6: 875-881, 2009.

van Norren D, and Gorgels TG. The action spectrum of photochemical damage to the retina: a review of monochromatic threshold data. *Photochemistry and photobiology* 87: 747-753, 2011.

Wang YV, Weick M, and Demb JB. Spectral and temporal sensitivity of cone-mediated responses in mouse retinal ganglion cells. *J Neurosci* 31: 7670-7681, 2011.

Weitz AC, Behrend MR, Lee NS, Klein RL, Chiodo VA, Hauswirth WW, Humayun MS, Weiland JD, and Chow RH. Imaging the retina's response to electrical stimulation with genetically encoded calcium indicators. *J Neurophysiol* 2013.

538 **Zariwala HA, Borghuis BG, Hoogland TM, Madisen L, Tian L, De Zeeuw CI, Zeng H,**
539 **Looger LL, Svoboda K, and Chen TW**. A Cre-dependent GCaMP3 reporter mouse for
540 neuronal imaging in vivo. *J Neurosci* 32: 3131-3141, 2012.

541

542

Figure 1

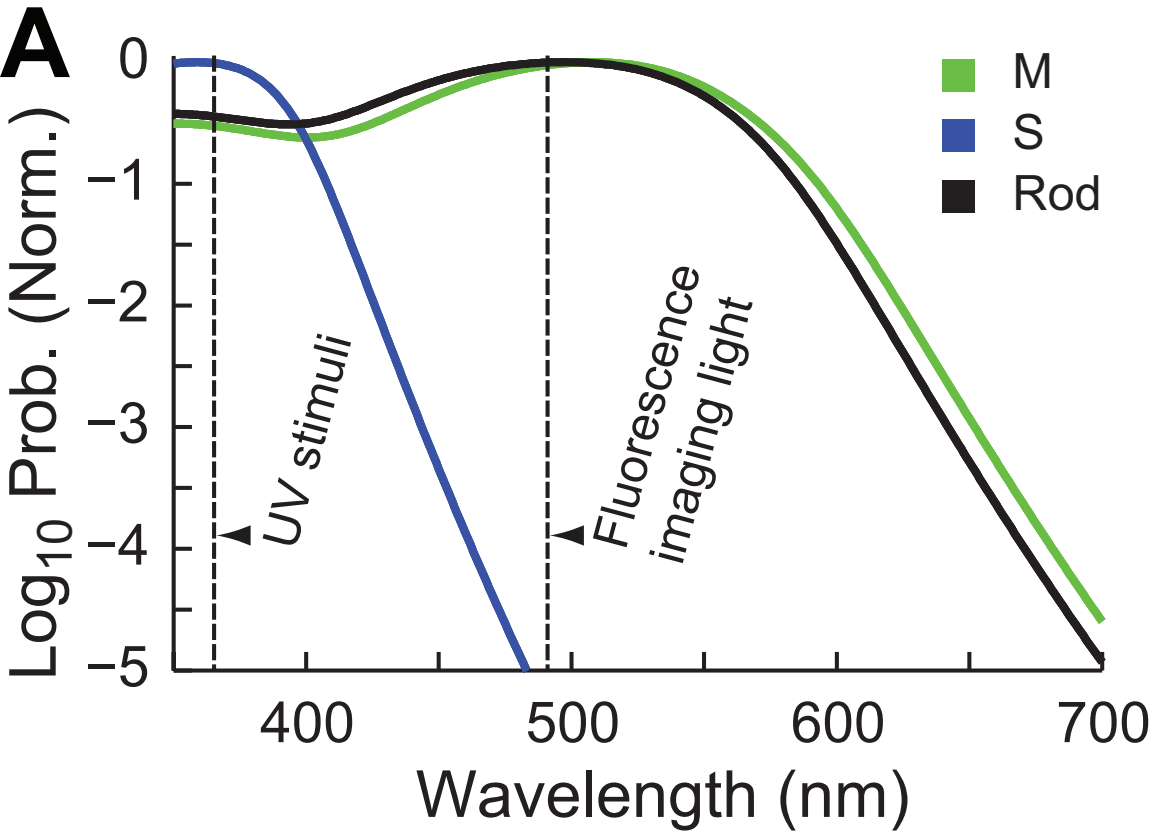
A
0
−1
−2
−3
−4
−5
Log10 Prob. (Norm.)
400
500
600
700
Wavelength (nm)
UV stimuli
Fluorescence imaging light
M
S
Rod

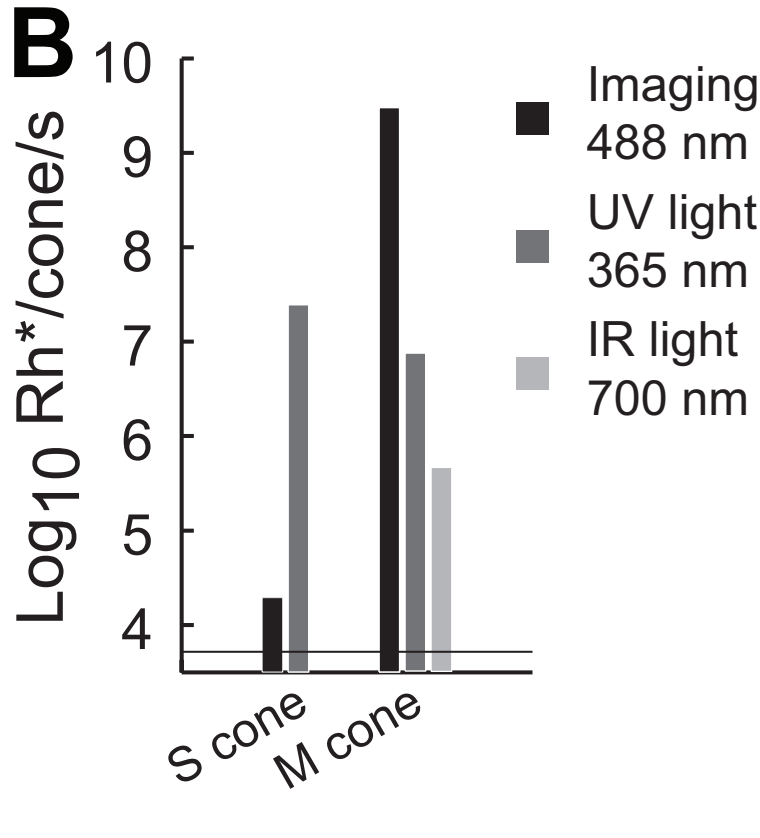
B
10
9
8
7
6
5
4
Log10 Rh*/cone/s
S cone
M cone
Imaging 488 nm
UV light 365 nm
IR light 700 nm

Figure 2

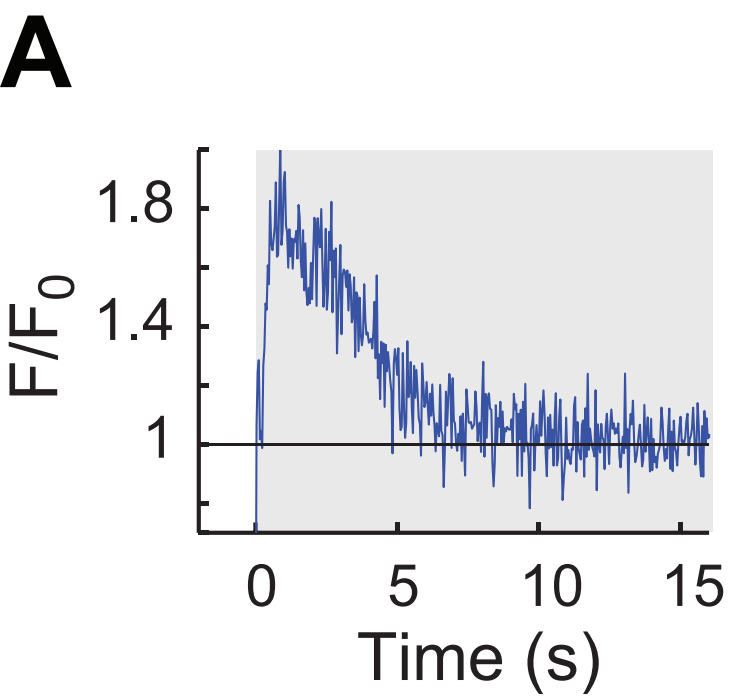

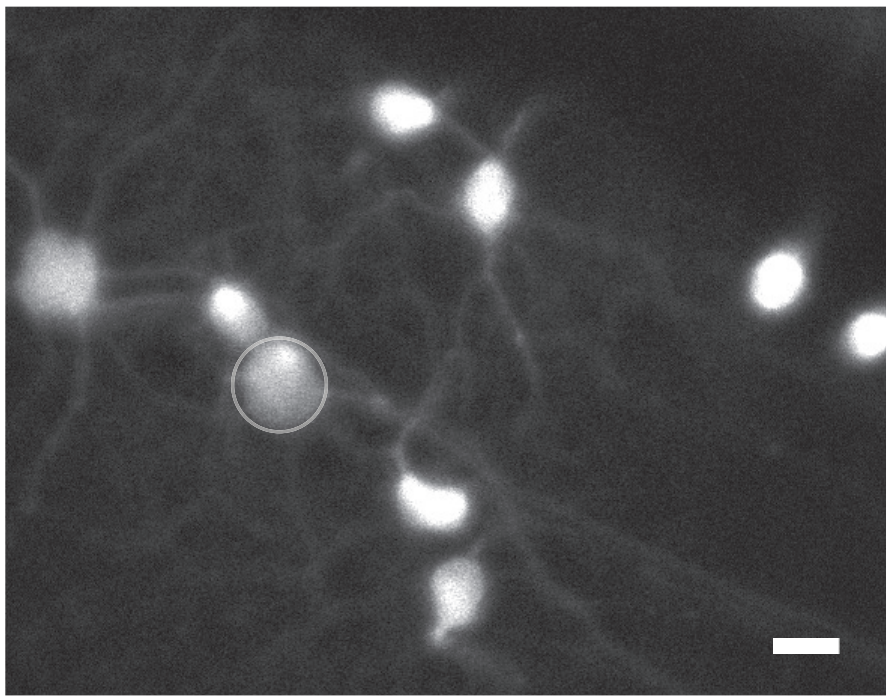

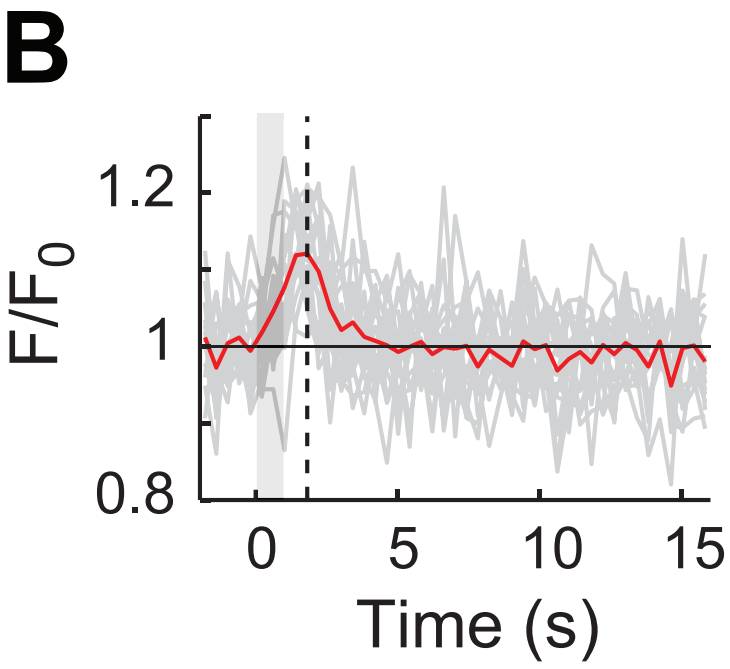

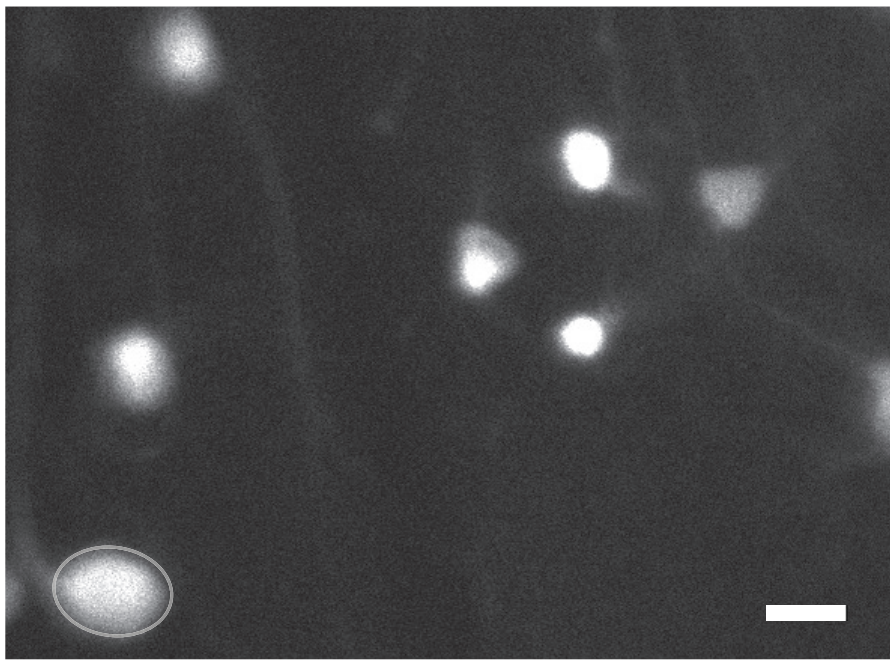

Figure 3

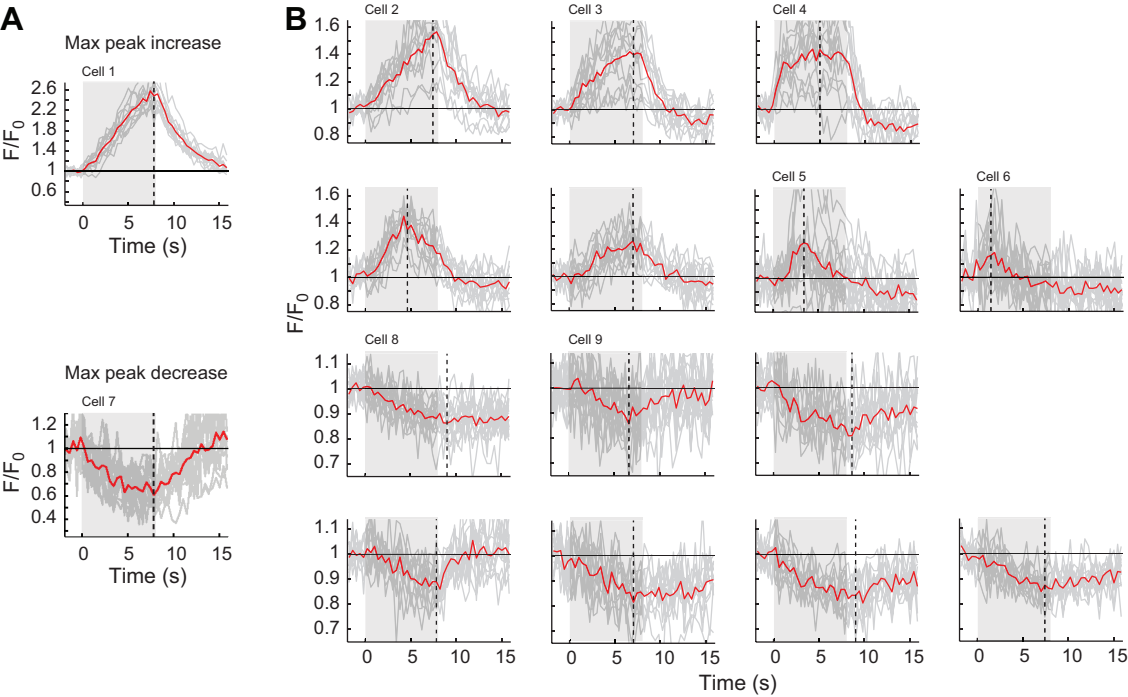
A
Max peak increase
Cell 1
F/F0
Time (s)
Max peak decrease
Cell 7
F/F0
Time (s)
B
Cell 2
Cell 3
Cell 4
Cell 5
Cell 6
Cell 8
Cell 9
F/F0
Time (s)

Figure 4

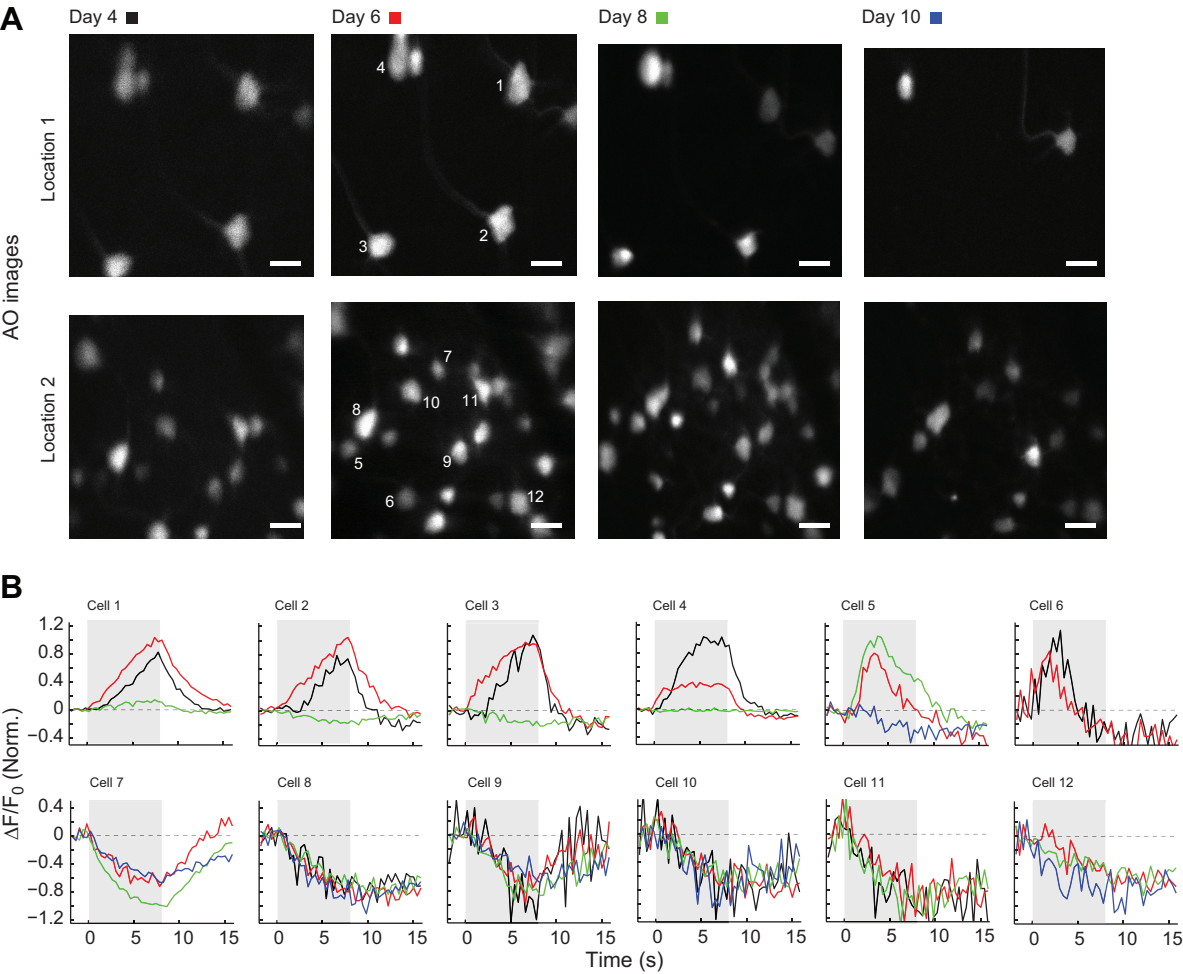
A
Day 4
Day 6
Day 8
Day 10
AO images
Location 1
Location 2
1
2
3
4
5
6
7
8
9
10
11
12
B
Cell 1
Cell 2
Cell 3
Cell 4
Cell 5
Cell 6
Cell 7
Cell 8
Cell 9
Cell 10
Cell 11
Cell 12
ΔF/F0 (Norm.)
Time (s)

Figure 5

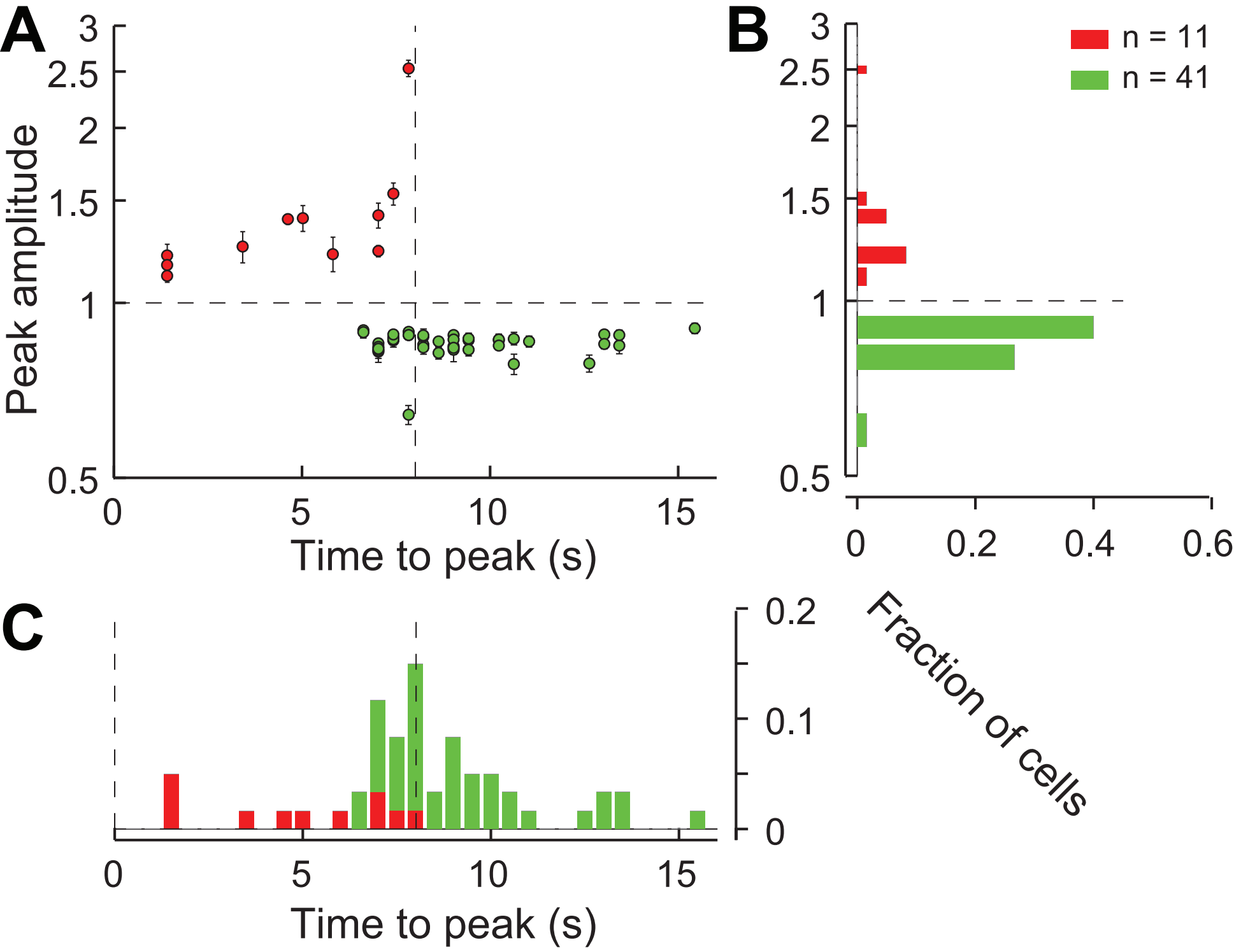
A
Peak amplitude
3
2.5
2
1.5
1
0.5
0
5
10
15
Time to peak (s)
B
n = 11
n = 41
0
0.2
0.4
0.6
C
0.2
0.1
0
Fraction of cells
0
5
10
15
Time to peak (s)